PROCEEDINGS OF SCIENCE

Shapes and sizes of diquarks in lattice QCD

Anthony Francis,[a,*] **Philippe de Forcrand,**[b] **Randy Lewis**[c] **and Kim Maltman**[c,d,e]

[a] *Institute of Physics, National Yang Ming Chiao Tung University, 30010 Hsinchu, Taiwan*

[b] *Theory Department, CERN, CH-1211 Geneva, Switzerland*

[c] *Department of Physics and Astronomy, York University, Toronto, Ontario, M3J 1P3, Canada*

[d] *Department of Mathematics and Statistics, York University, Toronto, Ontario M3J 1P3, Canada*

[e] *CSSM, University of Adelaide, Adelaide, SA, 5005, Australia*

E-mail: afrancis@nycu.edu.tw, forcrand@phys.ethz.ch, randy.lewis@yorku.ca, kmaltman@yorku.ca

The idea of diquarks as effective degrees of freedom in QCD has been a successful concept in explaining observed hadron spectra. Recently they have also played an important role in studying doubly heavy tetraquarks in phenomenology and on the lattice. The first member of this family of hadrons is the T_{cc}, newly discovered at LHCb. Despite their importance, the colored nature of diquarks has been an obstacle in lattice studies. We address this issue by studying diquarks on the lattice in the background of a heavy static quark, i.e. in a gauge-invariant formalism, with quark masses down to almost physical pion masses in full QCD.

We determine mass differences between different diquark channels as well as diquark-quark mass differences. Of particular interest are diquarks with "good" scalar, $\bar{3}_F$, $\bar{3}_c$, $J^P = 0^+$, quantum numbers. We find attractive quark-quark spatial correlations only in this channel and observe that the "good" diquark shape is spherical. From the spatial correlations in the "good" diquark channel we extract a diquark size of ~ 0.6 fm.

Our results provide quantitative support for modelling the low-lying baryon spectrum using good light diquark effective degrees of freedom.

41st International Conference on High Energy physics - ICHEP2022
6-13 July, 2022
Bologna, Italy

*Speaker

PoS(ICHEP2022)795

Diquarks as a concept [1] have a long history of successes in describing low-lying baryons and exotics. Experimental evidence, however, has been difficult to obtain. Formally their interpolating operator may be written as

$$D_\Gamma = q^c C\Gamma q' \tag{1}$$

where q, q' denote two different quark flavors, c, C indicate charge conjugation and Γ acts on Dirac space indices. A list of their possible quantum numbers is given in Tab. 1 (left).

One prediction of particular interest is that the special, so-called "good", $(\bar{3}_F, \bar{3}_c, J^P = 0^+)$ diquark configuration is attractive, see e.g. [2]. This implies it has the potential to produce an associated diquark substructure which could explain the pattern of observed states in the low-lying baryon spectrum. The binding energies of recently predicted doubly-heavy tetraquarks [3–15], can also be partially explained by this effect.

Even though diquarks are well founded in QCD, non-perturbative input through lattice simulations, is scarce. The reason is that they are not gauge-invariant, and the lattice cannot access them directly as a consequence. Here, we address this issue by forming gauge-invariant probes of diquark properties through embedding them in baryons together with a single static quark. The mass of this infinitely heavy quark cancels exactly in mass differences. Additionally, this configuration can be used to define a measure for the diquark structure through density-density correlations.

Our lattice simulations are performed with $n_f = 2 + 1$ dynamical quark ensembles generated by PACS-CS [16, 17] and available via the JLDG [18]. The lattice size is $L^3 \times T = 32^3 \times 64$ with lattice spacing $a = 0.090$ fm. The light sea quarks are an isospin doublet, denoted $\ell = u = d$. The strange quark, s, mass is held fixed near its physical value while the light quark mass is varied. The pion mass values are $m_\pi = 164,\ 299,\ 415,\ 575$ and 707 MeV. We also compare with new quenched simulations with a valence pion mass $m_\pi^v = 909$ MeV. All reported results are based on [19].

1. Diquark spectroscopy

To proceed we embed the diquark in a baryon containing a static quark Q, leading to the Euclidean-time-dependent correlator and a spectral decomposition of the form [20–23]:

$$C_\Gamma(t) = \sum_{\vec{x}} \left\langle [D_\Gamma Q](\vec{x}, t)\ [D_\Gamma Q]^\dagger(\vec{0}, 0) \right\rangle \sim \exp\left[-t\left(m_{D_\Gamma} + m_Q + O(m_Q^{-1})\right)\right] \ , \tag{2}$$

which provides a gauge-invariant probe of the mass differences of different diquark channels through the differences of the corresponding baryon masses, in which the mass of the static quark is exactly cancelled. The diquark-diquark and, similarly, diquark-quark, mass differences involving diquark pairs with flavors ud, ℓs $(\ell = u, d)$ and ss', where s' is an additional valence quark of mass m_s, can be accessed by taking the ratios of two diquark correlation functions, e.g. the "bad" $(\Gamma = \gamma_i)$ and the good $(\Gamma = \gamma_5)$, or a diquark and a static-light meson $(M_\Gamma = [\bar{Q}\Gamma q])$. These mass splittings are unique, non-perturbative features and can be viewed as fundamental characteristics of QCD [2].

The large range of pion masses enables short, controlled chiral extrapolations to the physical value of the pion mass.The results are summarised in Tab. 1 (right), which show the mass differences calculated in our lattice study compared to their phenomenological counterparts. Overall we observe very good agreement with phenomenological expectations, and confirm the special role of the attractive good diquark configuration.

J^P	C	F	Op: Γ
0^+	$\bar{3}$	$\bar{3}$	$\gamma_5, \gamma_0\gamma_5$
1^+	$\bar{3}$	6	γ_i, σ_{i0}
0^-	$\bar{3}$	6	$\mathbb{1}, \gamma_0$
1^-	$\bar{3}$	$\bar{3}$	$\gamma_i\gamma_5, \sigma_{ij}$

All in [MeV]	$\delta E_{\rm lat}(m_\pi^{\rm phys})$	$\delta E_{\rm pheno}$
$\delta(1^+ - 0^+)_{ud}$	198(4)	206(4)
$\delta(1^+ - 0^+)_{\ell s}$	145(5)	145(3)
$\delta(1^+ - 0^+)_{ss'}$	118(2)	
$\delta(Q[ud]_{0^+} - \bar{Q}u)$	319(1)	306(7)
$\delta(Q[\ell s]_{0^+} - \bar{Q}s)$	385(9)	397(1)
$\delta(Q[\ell s]_{0^+} - \bar{Q}\ell)$	450(6)	

Table 1: *(Left) Diquark operators and quantum numbers. The first row denotes the so-called "good", the second the "bad" and the final two the "not-even-bad" diquarks. (Right) Diquark-diquark (top rows) and Diquark-quark (bottom rows) mass differences. The phenomenological results are derived from [24]. Their errors are estimated via the difference between results including the charm and the bottom quark, respectively, while the central value is given by the bottom quark result.*

2. Diquark structure

Encouraged by this success, we study the spatial correlations of the quarks embedded in the static-light-light baryon with operator $B = [D_\Gamma Q]$. We define the quark density-density correlators

$$C_\Gamma^{dd}(\vec{x}_1, \vec{x}_2, t) = \left\langle B_\Gamma(\vec{0}, 2t)\rho(\vec{x}_1, t)\rho(\vec{x}_2, t)B_\Gamma^\dagger(\vec{0}, 0)\right\rangle \tag{3}$$

where $\rho(\vec{x}, t) = \bar{q}(\vec{x}, t)\gamma_0 q(\vec{x}, t)$, to study the diquark's internal structure via spatial correlations.

The static quark is set at the origin, while the light-quark source/sink points are located at $(\vec{0}, t_{src})$ and $(\vec{0}, t_{snk})$ with the inserted currents at $t_m = (t_{snk} + t_{src})/2$ with $(t_{snk} - t_{src}) = 16$. This maximises ground state saturation while keeping the noise low. We average over all spatial translations of the quark sources and sinks. The relative positions of the static source and current insertions $\vec{x}_1, \vec{x}_2$, can be understood in terms of $\vec{r}_{qq'} = \vec{x}_2 - \vec{x}_1$, $\vec{S} = (\vec{x}_1 + \vec{x}_2)/2$, i.e. the separation between the static source and diquark midpoint, in addition to the angle ϕ between $\vec{r}_{qq'}$ and $\vec{S}$. In the following we define the shorthand $\rho_2(r_{qq'}, S, \phi; \Gamma) \equiv C_\Gamma^{dd}(\vec{x}_1, \vec{x}_2, t_m)$, where the distance from the static source to the closer of the two insertion points is minimized for $\phi = \pi$ and maximized for $\phi = \pi/2$ for a fixed S and $r_{qq'}$. The static quark could potentially disrupt the diquark correlation if it gets too close. This disruption will be largest for the angle $\phi = \pi$ and smallest for $\phi = \pi/2$. We focus on these two limiting cases in the following. In the case of smallest disruption, the distance $|\vec{x}_1| = |\vec{x}_2| \equiv R$ and the angle Θ between $\vec{x}_1$ and $\vec{x}_2$ may be used to characterise the correlations. Introducing a further shorthand we write in the following $\rho_2^\perp(R, \theta) \equiv \rho_2(r_{qq'}, S, \pi/2)$ and $\rho_2^\parallel(r_{qq'}, S) \equiv \rho_2(r_{qq'}, S, \pi)$.

In the case of attraction in a given diquark channel we expect an increase in $\rho_2^\perp(R, \theta)$ with decreasing Θ at fixed R. We show the results for all available diquark channels in Fig. 1 (left) at a pion mass of 575 MeV. The angular variable $\cos(\Theta) = -1\,(+1)$ implies the quarks are opposite (on top) of each other, i.e. $\Theta = 180^\circ$ and 0°. We observe a clear increase exclusively in the good diquark channels $\Gamma = \gamma_5$ and $\gamma_5\gamma_0$. In all other channels we observe no indication of any such attraction.

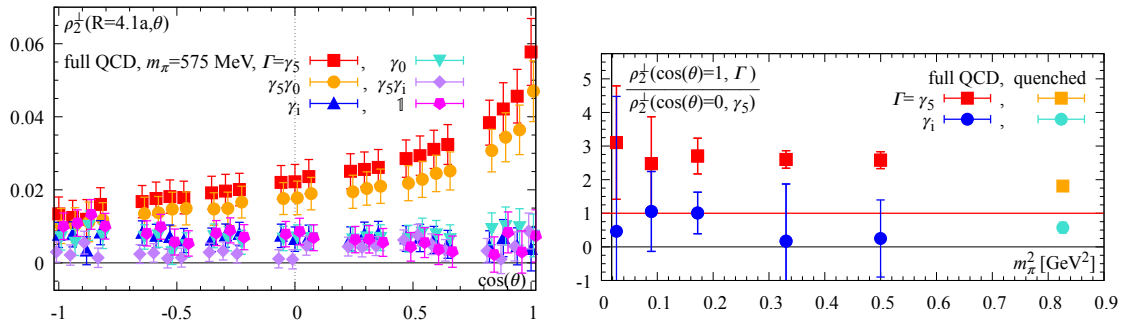

Figure 1: *Diquark attraction. (Left) The density-density correlators* $\rho_2^\perp(R = 4.1a, \Theta, \Gamma)$ *versus* $cos(\Theta)$ *at* $m_\pi = 575$ MeV. *(Right) The ratio* $\rho_2^\perp(R, \Theta = 0, \Gamma)/\rho_2^\perp(R, \Theta = \pi/2, \Gamma = \gamma_5)$ *versus* m_π^2. *Values above/below 1 for the red/blue points signal attraction in the good diquark that is absent for the bad diquark. The vertical line denotes physical* m_π.

In Fig. 1 (right) we study the quark mass dependence of this effect through the ratio between the results for $\Theta = 0°$ and 90°, i.e. $(\rho_2^\perp(R, \Theta = 0, \Gamma))/(\rho_2^\perp(R, \Theta = \pi/2, \gamma_5))$. Focusing on the good, $\Gamma = \gamma_5$, and bad, $\Gamma = \gamma_i$, channels, we observe the good channel exhibits a significantly increased ratio for all masses available while the bad diquark channel shows no sign of such an enhancement. These observations establish the attractive interaction in the good diquark channel.

Refining this picture of the good diquark, notice that the distance between the quarks in the probed diquark can be written as $r_{qq'} = R\sqrt{2(1 - \cos(\Theta))}$. Then we can re-interpret our results as

$$\rho_2^\perp(R, r_{qq'}) \sim \exp(-r_{qq'}/r_0) \ , \tag{4}$$

where we defined the diquark size parameter r_0 through the scale of the exponential decay of the spatial correlation between the two quarks q and q' constituting the diquark with $r_{qq'}$. Our results for all available R and m_π are shown in Fig.2 (left). Note that we do not see evidence for a distortion by the static quark as long as $r_{qq'} < R$. With the definition of the diquark size we perform a combined fit to all available R at a given value of m_π.

The results for $r_0(m_\pi^2)$ are displayed in Fig. 2 (top right), where we also compare with the results obtained in [21–23]. Overall we observe very good agreement with these previous studies and significantly extend them. Studying the decay of the spatial correlation between the quark-quark pair with distance we find the diameter of the diquark to be ~ 0.6 fm. A similar value was found in determinations of the size of mesons and baryon using a similar method in [25]. As such, the good diquark is of hadronic size.

Finally, we further study the good diquarks by comparing analogue definitions of the diquark sizes separately in the relative radial ($r_0^\parallel$, $\phi = \pi$) and tangential ($r_0^\perp$, $\phi = \pi/2$) orientations. This enables an estimation of the shape of the diquark and sheds light on possible polarisation effects through the static quark at the origin. The ratio $r_0^\perp/r_0^\parallel$ provides a measure of the diquark shape and the results shown in Fig. 2 (Bottom right) indicate $r_0^\perp/r_0^\parallel(m_\pi^2) \simeq 1$ within errors for all m_π. This implies that the diquarks have a near-spherical shape and that we do not observe polarisation effects due to the presence of the static quark.

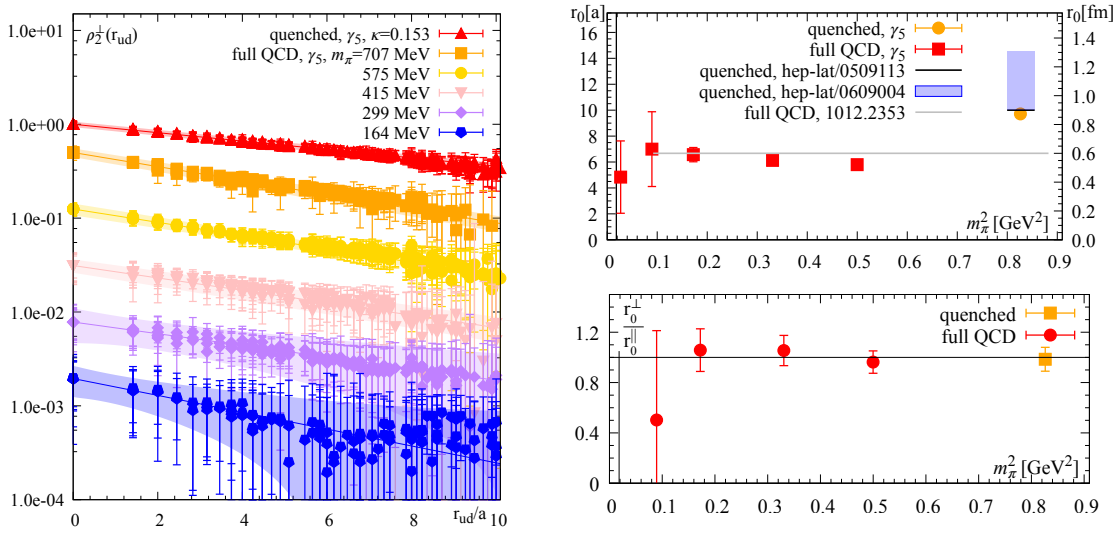

Figure 2: *Good diquark size. (Left) Exponential decay with $r_{qq'}$ of the density-density correlator $\rho_2^{\perp}(R,\Theta)$. Each m_π has its own color. Data sets are normalised at $r_{qq'} = 0$ and offset vertically. Results for all available R are shown together in one coloured set. Each coloured band comes from the combined fit used to determine the diquark size $r_0(m_\pi^2)$. (Top right) Resulting good diquark size r_0 versus m_π^2, compared to results from the literature. The vertical line denotes physical m_π. (Bottom right) Good diquark shape. The ratio $r_0^{\perp}/r_0^{\parallel}$ as a function of m_π. The vertical line denotes physical m_π.*

3. Discussion and Summary

We presented results on both diquark spectroscopy and diquark structure, using ab initio lattice QCD simulations. By embedding the diquarks in baryons together with a single static quark we formed gauge-invariant probes of their properties. Evaluating diquark-diquark and diquark-quark mass differences in which the static spectator quark mass cancels out exactly we observe very good agreement for all available mass splittings when comparing with phenomenological estimates. The splittings confirm the special status of the good diquark, where we observe a relative mass difference of 198(4) MeV compared to the bad diquark at the physical pion mass point.

By studying density-density correlations we found further strong evidence for quark-quark attraction in the good diquark channel. This compact spatial correlation was seen only in the good diquark channel providing clear support for the good diquark picture. We observed that the good diquark diameter defined through this spatial correlation is $r_0 \simeq O(0.6)$ fm. This implies diquarks are similar in size to mesons and baryons [25]. Finally we probed the shape of the good diquark by evaluating the ratio of its tangential and radial sizes. Our results imply an almost spherical shape, with no discernible evidence for polarisation induced by the static spectator quark.

Diquarks play an important role as possible building blocks of exotic hadrons. Together with new insights from theory, upcoming experiments at LHCb, Belle-II, BESIII, JLab, J-Parc and also EIC will add new results to hadron spectroscopy with heavy quarks and refine our understanding of how hadrons are formed.

Further details and supporting studies that go beyond the scope of this contribution can found in [19]. The results shown here were taken from this main reference.

Acknowledgements

The authors acknowledge the support by the high performance computing resources Niagara maintained by SciNet and Compute Canada as well as HPC-QCD by CERN. RL and KM acknowledge the support of grants from the Natural Sciences and Engineering Research Council of Canada.

References

[1] D.B. Lichtenberg and L.J. Tassie, *Phys. Rev.* **155** (1967) 1601.
[2] R. Jaffe, *Phys. Rept.* **409** (2005) 1 [hep-ph/0409065].
[3] A. Francis, R.J. Hudspith, R. Lewis and K. Maltman, *Phys. Rev. Lett.* **118** (2017) 142001 [1607.05214].
[4] M. Karliner and J.L. Rosner, *Phys. Rev. Lett.* **119** (2017) 202001 [1707.07666].
[5] E.J. Eichten and C. Quigg, *Phys. Rev. Lett.* **119** (2017) 202002 [1707.09575].
[6] A. Czarnecki, B. Leng and M.B. Voloshin, *Phys. Lett. B* **778** (2018) 233 [1708.04594].
[7] A. Francis, R.J. Hudspith, R. Lewis and K. Maltman, *Phys. Rev. D* **99** (2019) 054505 [1810.10550].
[8] R.J. Hudspith, B. Colquhoun, A. Francis, R. Lewis and K. Maltman, *Phys. Rev. D* **102** (2020) 114506 [2006.14294].
[9] P. Junnarkar, N. Mathur and M. Padmanath, *Phys. Rev. D* **99** (2019) 034507 [1810.12285].
[10] European Twisted Mass collaboration, *Phys. Rev. D* **87** (2013) 114511 [1209.6274].
[11] P. Bicudo, K. Cichy, A. Peters and M. Wagner, *Phys. Rev. D* **93** (2016) 034501 [1510.03441].
[12] P. Bicudo, K. Cichy, A. Peters, B. Wagenbach and M. Wagner, *Phys. Rev. D* **92** (2015) 014507 [1505.00613].
[13] P. Bicudo, J. Scheunert and M. Wagner, *Phys. Rev. D* **95** (2017) 034502 [1612.02758].
[14] P. Bicudo, A. Peters, S. Velten and M. Wagner, 2101.00723.
[15] L. Leskovec, S. Meinel, M. Pflaumer and M. Wagner, *Phys. Rev. D* **100** (2019) 014503 [1904.04197].
[16] PACS-CS collaboration, *Phys. Rev. D* **79** (2009) 034503 [0807.1661].
[17] PACS-CS collaboration, *Phys. Rev. D* **87** (2013) 094512 [1301.4743].
[18] JLDG, *Ensembles available from https://www.jldg.org* .
[19] A. Francis, P. de Forcrand, R. Lewis and K. Maltman, *JHEP* **05** (2022) 062 [2106.09080].
[20] K. Orginos, *PoS* **LAT2005** (2006) 054 [hep-lat/0510082].
[21] C. Alexandrou, P. de Forcrand and B. Lucini, *PoS* **LAT2005** (2006) 053 [hep-lat/0509113].
[22] C. Alexandrou, P. de Forcrand and B. Lucini, *Phys. Rev. Lett.* **97** (2006) 222002 [hep-lat/0609004].
[23] J. Green, J. Negele, M. Engelhardt and P. Varilly, *PoS* **LATTICE2010** (2010) 140 [1012.2353].
[24] Particle Data Group collaboration, *PTEP* **2020** (2020) 083C01.
[25] B. Blossier and A. Gérardin, *Phys. Rev. D* **94** (2016) 074504 [1604.02891].